Letter

Hard x-ray intensity autocorrelation using direct two-photon absorption

Taito Osaka,[1,*] Ichiro Inoue,[1] Jumpei Yamada,[1] Yuichi Inubushi,[1,2] Shotaro Matsumura,[3] Yasuhisa Sano,[3] Kensuke Tono,[1,2] Kazuto Yamauchi,[3,4] Kenji Tamasaku,[1] and Makina Yabashi[1,2]

[1]*RIKEN SPring-8 Center, 1-1-1 Kouto, Sayo-cho, Sayo-gun, Hyogo 679-5148, Japan*

[2]*Japan Synchrotron Radiation Research Institute, 1-1-1 Kouto, Sayo-cho, Sayo-gun, Hyogo 679-5198, Japan*

[3]*Division of Precision Engineering and Applied Physics, Graduate School of Engineering, Osaka University, 2-1 Yamada-oka, Suita, Osaka 565-0871, Japan*

[4]*Research Center for Precision Engineering, Graduate School of Engineering, Osaka University, 2-1 Yamada-oka, Suita, Osaka 565-0871, Japan*

(Received 15 September 2020; revised 27 January 2022; accepted 9 February 2022; published 18 March 2022)

An intensity autocorrelation measurement is demonstrated to characterize a pulse duration of 9-keV x-ray free-electron laser (XFEL) pulses from a split-delay optical (SDO) system with four-bounce silicon 220 reflections in each branch. XFEL pulse replicas with variable time delays are generated by the SDO system itself. High intensity of $>2 \times 10^{16}\,\mathrm{W/cm^2}$ achieved in a self-seeding operation and careful data analysis allow the measurement with direct two-photon absorption. The autocorrelation trace gave a duration of 7.6 ± 0.8 fs in full width at half maximum for a Gaussian assumption. Furthermore, the trace shows good agreement with a simulation of the XFEL pulse shape propagating through the SDO system, irrespective of spectral chirps in the original XFEL pulses. Our results open the door toward direct temporal characterization of narrowband XFELs at the hard x-ray regime, such as self-seeded and future cavity-based XFELs, and indicate a solid way for temporal tailoring of ultrafast x-ray pulses with perfect crystals.

DOI: 10.1103/PhysRevResearch.4.L012035

I. INTRODUCTION

Hard x-ray free-electron lasers (XFELs) [1–5] generated in the self-amplified spontaneous emission (SASE) scheme [6] with remarkable optical properties have opened up unique opportunities in various scientific fields, such as pump-probe studies of atomic-scale photoinduced dynamics in matter on femtosecond timescales [7,8] and observation or application of nonlinear optical processes in the hard x-ray regime [9,10]. The pulse duration as well as temporal profile of XFEL pulses is essential information for extracting accurate physical quantities, e.g., frequencies and lifetimes of dynamic processes and efficiencies of nonlinear x-ray–matter interactions.

To characterize the pulse duration of ultrafast optical lasers, intensity autocorrelation [11] is the most classical and popular technique from the infrared to extreme ultraviolet spectral regimes [12]. In this scheme, two pulse replicas with variable time delays generated in a split-delay optical (SDO) system are mixed on a nonlinear medium. Then the nonlinearity of, for example, second-harmonic generation (SHG) [13] or two-photon absorption (TPA) [14] is measured as a function of the time delay τ. The trace directly relates to the temporal autocorrelation function of the laser pulse $\int I(t)I(t-\tau)dt$, giving an estimate of the pulse duration. This technique covers a broad range of timescales below subnanoseconds, which is inaccessible by fast diodes. The time resolution is, in principle, defined as the lifetime of intermediate states in the nonlinear process, which is typically a few femtoseconds at the visible regime ($E_\omega \sim 1$ eV where E_ω is the photon energy) and shorter at higher photon energies. Furthermore, the technique has been extended to the so-called frequency-resolved optical gating (FROG) [15], which is a full temporal characterization method capturing spectrograms of nonlinear signals.

For the hard x-ray regime, however, intensity autocorrelation has not been realized because of the extremely low efficiencies in nonlinear optical processes and the lack of SDO systems. For the former, x-ray nonlinear processes have been reported with a tightly focused XFEL at an extreme intensity of 10^{18} to $10^{20}\,\mathrm{W/cm^2}$ [9,10,16–19]. Remarkable efforts in establishing experimental setups and data analyses have made it possible to observe x-ray SHG [20] and TPA [21] at a moderate intensity of $<10^{17}\,\mathrm{W/cm^2}$ by accumulating a large number of shots to compensate for the low signal rates ($\sim 10^{-3}$ counts/shot). Still, a threshold in intensity is set at $\sim 10^{16}\,\mathrm{W/cm^2}$ for practical observations. For the latter, x-ray SDO systems with silicon (Si) 220 reflection have been made available recently [22–24], implemented mainly for unveiling atomic-scale fluctuation in disordered systems at subpicosecond to nanosecond timescales [25,26]. However, intensity autocorrelation has not been achieved yet, due to the following bottlenecks. First is a relative bandwidth of current SDO systems $\Delta E/E_\omega \sim 5.6 \times 10^{-5}$, which is much narrower than that of SASE XFELs ($\Delta E/E_\omega \sim 3 \times 10^{-3}$ to 5×10^{-3}). The unmatched bandwidth leads to a considerable loss of x-ray flux through the SDO system. Second is the

*osaka@spring8.or.jp

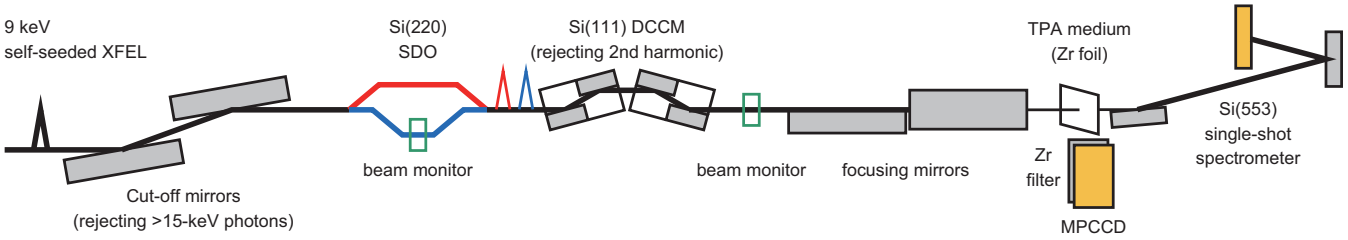

FIG. 1. Schematic illustration of the setup (not scaled). See text for details.

difficulty in combining an SDO system with a nanofocusing one often used in the study of nonlinear x-ray processes because extraordinary stability is required on both systems. These facts have limited intensity of split XFEL pulses to, typically, $\sim 10^{15}\,\mathrm{W/cm^2}$ that is far from the threshold.

So far, pulse durations of XFELs have been indirectly estimated from the following information: fine structures in XFEL spectra [27,28], number of longitudinal modes [29], electron bunch profiles [30,31], and degree of longitudinal coherence of fluorescent x rays [32]. However, these approaches entail nontrivial assumptions of the temporal shape or parameters in FEL simulations. Although angular streaking of photoelectrons [33] is a direct and model-free technique, it is available only $\lesssim 2$ keV in the soft x-ray regime because of the low photo-absorption coefficients of target gasses for hard x rays.

In this paper, we report an intensity autocorrelation measurement for 9-keV XFELs with the help of a self-seeding amplification [34,35], which enhances the intensity of split XFEL pulses from a Si(220) SDO system by a factor >5 and achieves the threshold intensity at a micrometer-scale focal size. We apply TPA for the nonlinear process. An advantage of TPA against SHG is that any phase-matching conditions with severe alignment for the nonlinear medium are not required. An autocorrelation trace clearly presents a peak around $\tau = 0$ fs. The trace gives a pulse duration of 7.6 ± 0.8 fs in full width at half maximum (FWHM) for a Gaussian assumption and shows good agreement with a simulated temporal shape of the XFEL pulse after the SDO system.

II. EXPERIMENTAL SETUP

Figure 1 shows a schematic layout of the experimental setup. Split XFEL pulses from an SDO system are focused to a micrometer spot and spatially merged collinearly on a nonlinear medium for TPA. In the TPA process, a K-shell electron with a binding energy of $<2E_\omega$ and $>E_\omega$ is excited by absorbing two photons across a virtual intermediate state with a typical lifetime of <1 as. Then the core hole is filled by outer-shell electrons while emitting fluorescent x rays as nonlinear signals. The signals are collected through a spectrometer placed at 90° in the polarization plane of the XFEL to suppress the detection of elastically scattered photons from the medium. At a low signal rate in this paper, it is necessary to reject high-order harmonic radiation of XFEL because it can create background signals through a one-photon absorption (OPA) process.

The experiment was performed at BL3 of SPring-8 Angstrom Compact free-electron LAser (SACLA) [36] operated at a repetition rate of 60 Hz. A brilliant 9-keV XFEL pulse was generated in a reflection self-seeding scheme [35,37] and split into two pulses by a Si(220) SDO system operating in a wavefront division mode [42]. The SDO system provides a broad range of time delays up to ~ 200 ps with subfemtosecond accuracy. The split pulses were focused to 1.0 (horizontal) $\times$ 0.6 (vertical) $\mu\mathrm{m}^2$ in FWHM by Kirkpatrick-Baez mirrors [44]. Shot-to-shot pulse energies of the two branches (I_1 and I_2) and the sum of them ($I_{\mathrm{sum}} = I_1 + I_2$) were measured with noninvasive beam monitors implemented in the SDO system and the beamline, respectively [37]. We used a 20-μm-thick zirconium (Zr) foil as the TPA medium with a K-shell binding energy of 18 keV. The foil was tilted 30° from the normal incidence and scanned to illuminate fresh area for every shot. The TPA signal, Zr $K\alpha$ fluorescence at 16 keV in this experiment, was measured by a multi-port charge-coupled device (MPCCD) [45], which covered a solid angle of 1.0×10^{-2} sr with an energy resolution of 0.2 keV root-mean-square (rms). A 75-μm Zr filter was placed in front of the MPCCD to reduce elastic scattering of 9-keV photons with transmittance of 0.9%, while it was 37% for the TPA signal. A two-bounce total reflection mirror with a cutoff energy of 15 keV and a Si(111) double channel-cut monochromator (DCCM) [46] were utilized to reduce the harmonic radiation. In addition, as complementary information of temporal properties, shot-to-shot spectra of the split beams were measured by a dispersive spectrometer [27] with a Si(553) flat-crystal analyzer of which energy range and resolution were ~ 5 eV and 40 meV/pixel, respectively.

III. DATA ANALYSIS

Before data analysis, influence of unbalanced intensities of the split beams is estimated because the intensity ratio between the subpulses is highly sensitive to the pointing of the incoming XFEL pulse in the wavefront division mode [42]. By assuming an identical temporal shape for the subpulses and neglecting interfering terms, the delay-time dependent TPA intensity $I_{\mathrm{TPA}}(\tau)$ may be written by

$$I_{\mathrm{TPA}}(\tau) \propto I_1^2 + I_2^2 + 4g_2(\tau) \int I_1(t) I_2(t) dt, \qquad (1)$$

where $g_2(\tau)$ is the normalized autocorrelation function defined as

$$g_2(\tau) = \frac{\int I_{\mathrm{split}}(t) I_{\mathrm{split}}(t-\tau) dt}{\int I_{\mathrm{split}}(t) I_{\mathrm{split}}(t) dt}. \qquad (2)$$

Here, $I_{\rm split}(t)$ denotes either $I_1(t)$ or $I_2(t)$. Introducing a normalized difference of the pulse energy $R = (I_1 - I_2)/I_{\rm sum}$, we finally obtain

$$I_{\rm TPA}(\tau) \propto \frac{[1 + 2g_2(\tau)] + [1 - 2g_2(\tau)]R^2}{3} I_{\rm sum}^2. \quad (3)$$

At $R = 0$, $I_{\rm TPA}(\tau)$ corresponds to the ideal autocorrelation trace with a peak-to-base (PB) ratio of 3. In contrast, the PB ratio decreases as $|R|$ increases, expressed by PB ratio $= (3 - R^2)/(1 + R^2)$. In the following data analysis, we only utilized selected shots with $|R| < 0.3$ to reduce the deviation of TPA intensity from that at $R = 0$ while keeping sufficient statistics. A mean value of $|R|$ was 0.14 over the selected shots, which provides small deviations of 0.7 and 2% for the peak and base values, respectively.

Next, we differentiate the TPA signal from the background, which was mainly composed of cosmic rays, elastic scattering of 9-keV photons, and fluorescence generated by high-order harmonic radiation through OPA, as the following procedures. First, MPCCD data were analyzed by a droplet algorithm [37,47], in which analog-to-digital readouts of neighboring pixels with that above a threshold were summed up, and then the readout of a single droplet, which is a cluster of summed pixels, was converted to the photon energy. Through the droplet analysis, cosmic rays were well extracted because they create wider droplets with much higher photon energies than the TPA signal. Figure 2(a) represents converted spectra, which show three peaks at (E) 9 keV, (F) 16 keV, and (P) 18 keV. The peak (E) corresponds to elastic scattering of 9-keV photons and the peak (F) Zr $K\alpha_1$ and $K\alpha_2$ fluorescence at 15.775 and 15.691 keV, respectively. The peak (P) may contain pileup of two 9-keV photons detected in a single droplet and weak $K\beta$ fluorescence at 17.668 keV.

Since $K\alpha$ fluorescence generated by the high-order harmonics cannot be differentiated from the TPA signal through the droplet analysis, the harmonics were reduced to $\sim$1.0 photon shot^{-1} μJ^{-1} in this paper. Note that the third harmonic mainly contributed, while the others were negligibly small. Residual harmonic radiation can still generate $K\alpha$ fluorescence of 4.7×10^{-5} counts shot^{-1} μJ^{-1}, which was sufficiently smaller than that of a measured signal rate, as shown in Fig. 2(b). Elastically scattered harmonic photons could also generate $K\alpha$ fluorescence from the filter located in front of the MPCCD, whereas the rate was estimated to be $<1 \times 10^{-8}$ counts shot^{-1} μJ^{-1}.

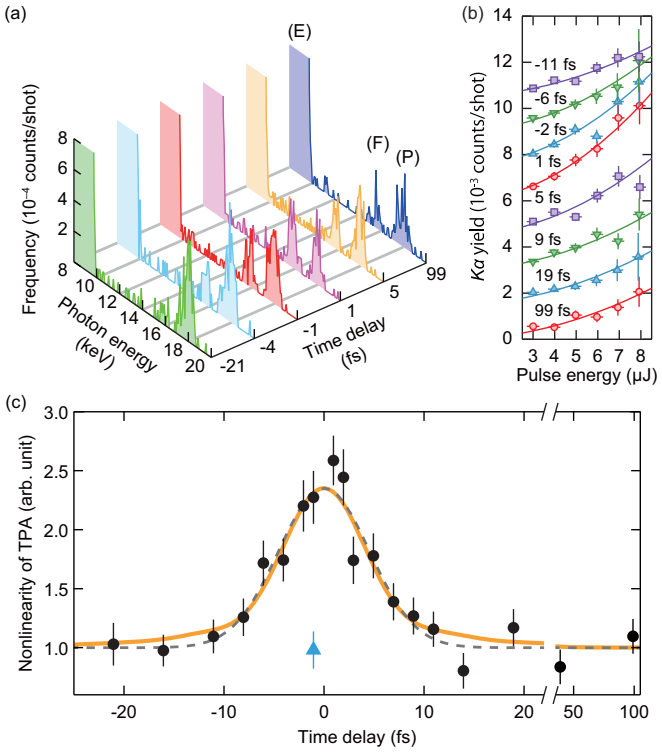

FIG. 2. (a) Converted spectra for $6.5\,\mu{\rm J} < I_{\rm sum} < 8.5\,\mu{\rm J}$. The peak (E) at 9 keV is over the range. (b) Pulse-energy dependence of $K\alpha$ yields. Each plot is separated from the others by adding a vertical offset. Error bar represents the statistical error. Solid line is the fitted quadratic function at each delay. (c) Delay-time dependence of the nonlinearity of two-photon absorption (TPA; circle), which is normalized by the base value of the fitted Gaussian. The triangle point represents the nonlinearity measured with spatially separated beams. Error bar is the fitting error. Dashed and solid lines show the fitted Gaussian and the autocorrelation function of a simulated pulse shape (shown in Fig. 4), respectively.

IV. RESULTS AND DISCUSSION

A. Autocorrelation trace

The pulse-energy dependence of $K\alpha$ yield, collected over a photon energy range from 14.74 to 16.68 keV, was analyzed at various time delays [Fig. 2(b)]. At each delay, >0.4 M shots were accumulated, and $\sim$40% of the total shots fell in $I_{\rm sum}$ ranging from 2.5 to 8.5 μJ ($\sim 2 \times 10^{16}$ to 8×10^{16} W/cm^2) were utilized [37]. This limitation eliminated misfires of the self-seeding amplification [Fig. 3(e)] of which spatiotemporal profiles at the sample were possibly deformed. Each curve of $K\alpha$ yield was fitted by a quadratic function described by $y = ax^2 + bx$. The quadratic and linear terms are contributed to TPA by the fundamental and OPA by the harmonics, respec-

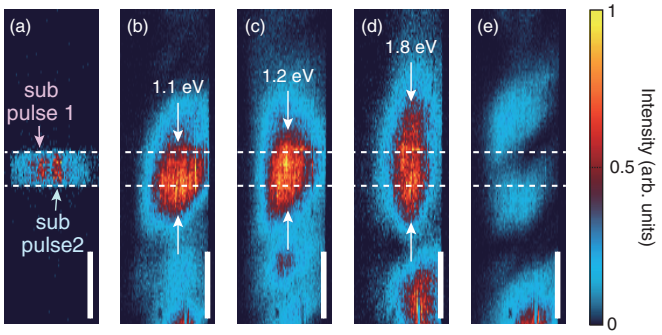

FIG. 3. Examples of single-shot spectra of (a) the split pulses and (b)–(e) the original self-seeded XFEL pulses in a 4-eV range. Vertical and horizontal axes represent the photon energy and spatial position along the horizontal direction, respectively. Scale bar denotes 1 eV. Dashed line shows the spectral range of 0.5 eV reflected by the split-delay optical (SDO) system. The self-seeding amplification was successful for (b)–(d) but misfired for (e).

tively. Here, b was fixed to 4.7×10^{-5} counts shot^{-1} μJ^{-1}, which was expected from the number of residual harmonics, as described before.

The nonlinearity of TPA a is plotted as a function of τ in Fig. 2(c) (circle). The plot displays a peak around $\tau = 0$ fs and almost constant base at $|\tau| > 20$ fs. The validity of the base value was confirmed from the fact that a similar value was obtained with split beams intentionally separated in space (triangle), which is analogous to the temporal separation ($\tau = \infty$) and insensitive to pointing fluctuation. The dashed line in Fig. 2(c) represents the best fit of a Gaussian. The PB ratio is 2.3, whereas the ideal value is 3. This discrepancy was mainly attributed to the spatial mismatch between the two beams due to the relative pointing fluctuation of ~0.1 μm rms and the slow drift of ~0.2 μm/h. Note that the SDO system was adjusted at every time delay to correct the drift. By assuming a Gaussian profile, the FWHM duration is estimated to be 7.6 ± 0.8 fs, which compares the value of 6–7 fs reported for a self-seeded beam propagating through a Si(111) monochromator [48]. The small discrepancy could originate in the difference in bandwidth between the Si 111 and 220 reflections, as discussed later.

B. Temporal deformation through Bragg diffraction

Here, we discuss the influence of the monochromatization by the crystal optics employed in the Si(111) DCCM and the SDO system. In general, the pulse duration could be widened by the monochromatization, following the Fourier-transform relationship between time and frequency. However, if the incident pulse is highly chirped and its duration is much longer than the Fourier-limited one, the pulse duration might be shortened because only a part of temporal components in the incident wave satisfies the Bragg condition. We investigate these effects by a numerical simulation based on a Fourier-transform analysis. A temporal shape of x rays reflected by the crystal optics may be expressed by [43]

$$I_{\rm out}(t) = \left| \int E_{\rm in}(\omega) R^4_{111}(\omega) R^4_{220}(\omega) \exp(i\omega t) d\omega \right|^2, \quad (4)$$

where $E_{\rm in}(\omega)$ is the slowly varying complex amplitude in the frequency domain of the input wave that corresponds to the original XFEL pulse and $R^4_{111}(\omega)$ [$R^4_{220}(\omega)$] complex amplitude ratio for the Bragg diffraction in the DCCM (SDO system). Since we can regard that all the crystals have perfect crystallinity [40,46], we applied theoretical curves calculated with dynamical theory of x-ray diffraction [49] to $R_{111}(\omega)$ and $R_{220}(\omega)$. In fact, the spectrum of the split beam [Fig. 3(a)] was in good agreement with the theoretical one.

Regarding $E_{\rm in}(\omega)$, the amplitude was measured by retracting the DCCM and SDO system [Figs. 3(b)–3(e)], although the phase was lost. Thus, only the phase of $E_{\rm in}(\omega)$ is the unknown parameter to simulate $I_{\rm out}(t)$. One of remarkable features on the measured spectra is that the seeded part contained a single spike of 1.0–1.8 eV in FWHM, which is wider than that of the seeding source of 0.5 eV from a Si(220) monochromator. This spectral broadening may have occurred during the amplification process by energy chirps in the electron bunches [35]. Therefore, it is reasonable that the pulse duration of the input beam was longer than the Fourier-limited one of 1.8 fs for 1-eV bandwidth, due to spectral chirps in $E_{\rm in}(\omega)$. For performing the simulation, we assumed $E_{\rm in}(\omega)$ with the following constraints: (1) the FWHM bandwidth is 1.0–1.8 eV as measured, and (2) the temporal shape is expressed by a Gaussian with an FWHM of 6 fs as reported previously [31]. We created 500 datasets for $E_{\rm in}(\omega)$ while satisfying the above constraints and simulated $I_{\rm out}(t)$ [37]. The black line in Fig. 4 represents $I_{\rm out}(t)$ averaged over the 500 shots. The profile $I_{\rm out}(t)$ with a 7.4-fs peak and an oscillatory tail after the main peak is consistent with the impulse response where $E_{\rm in}(\omega)$ has infinite bandwidth on a constant phase. The tail is attributed to multiple diffraction in the perfect crystals [43]. Note that single-shot shapes (gray) are like each other, irrespective of the phase of $E_{\rm in}(\omega)$, indicating that the output shape is mainly determined by $R_{220}(\omega)$. Therefore, this simulation provides a realistic temporal shape of the split XFEL pulses, which is supported by the autocorrelation trace shown in Fig. 2(c). Furthermore, this is the first experimental observation of the temporal deformation through Bragg diffraction, leading to a solid way for temporal tailoring of fluctuating x-ray pulses with perfect crystals. In contrast, this characteristic also denotes that the time resolution of this technique is set by the impulse response of the SDO system in addition to the lifetime of the intermediate state. To characterize XFELs with a short pulse duration, one needs to employ an SDO system with a wider bandwidth than that of the target pulse. Thus, it is needed to exploit total-reflection or multilayer-coated mirrors [50] with a relative bandwidth of, typically, >1% for SASE and attosecond XFELs [51]. It should, however, be noted that the current system could work well for future cavity-based XFELs with a bandwidth of the order of 10 meV [52,53] that is much narrower than the Si(220) bandwidth.

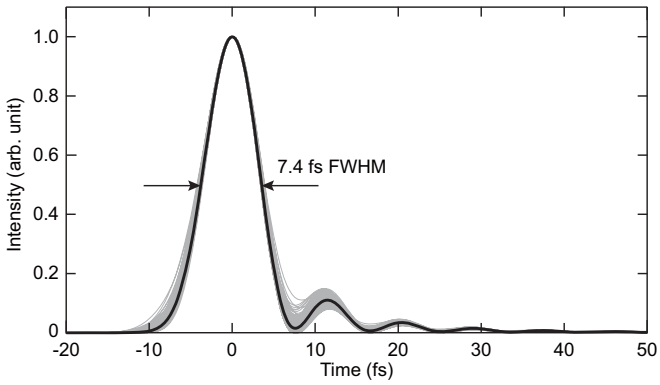

FIG. 4. Simulated x-ray free-electron laser (XFEL) pulse shapes $I_{\rm out}(t)$. Black line represents the average over 500 simulated shapes (gray). Each shape is normalized by the peak value. The full width at half maximum (FWHM) duration of the main peak distributed from 7.2 to 7.8 fs in the simulation.

C. Future improvements of TPA intensity autocorrelation method

Next, we discuss future improvements. One of drawbacks of this paper is the long data collection time (>37 h for accumulating ~8 M shots at the repetition rate of 60 Hz). Since the TPA cross-section may scale as Z^{-6} [18], where Z is the

nuclear charge, the signal rate can be increased by using low-Z materials as the TPA medium. For example, the cross-section of zinc ($Z = 30$ with a K-shell binding energy of 9.7 keV) is estimated to be 5 times higher than that of Zr ($Z = 40$) used in this paper, although it could impose the use of a sophisticated spectrometer with a higher energy resolution than MPCCD, e.g., a spherically bent crystal spectrometer operating in the Johann [54] or Johansson [55] geometries and a superconducting transition-edge sensor [56]. In addition, recent advances in x-ray focusing systems with high stability [57] will allow for the combinative use of nanofocusing optics and an SDO system, which enhances intensity by a factor >100. Increasing the repetition rate of the XFEL source is also straightforward to reduce the data collection time. High-repetition-rate XFEL facilities being available recently, such as the European XFEL, enable a similar measurement within a few minutes, whereas one needs to manage the high heat load on optics up to 1 kW and to implement an ultrafast sample delivery system (>20 m/s for >20-μm separation at a repetition rate of 1 MHz).

D. Possibilities of advanced autocorrelation techniques

Finally, we discuss the possibilities of advanced autocorrelation techniques, such as single-shot, background-free, and/or model-free full-temporal characterization. Although the intensity autocorrelation technique can be extended to the well-established single-shot metrology where the delay information is encoded in space [58], it requires at least 5 or 6 orders of magnitude higher count rates than that obtained in this paper, i.e., $>10^2$–10^3 counts/shot. Such a count rate is still challenging even with the improvements mentioned above and needs to seek much more efficient nonlinear processes than TPA. The two other techniques are based on a phase-sensitive nonlinear process, such as SHG. Although the narrow phase-matching condition at the hard x-ray regime [20] makes the measurement challenging, it may allow for the elimination of background signals generated from the individual pulse replicas at a crossing geometry with a small crossing angle of submilliradians, reducing the uncertainty of the autocorrelation trace at the tail specifically. The background-free SHG intensity autocorrelation technique can be extended to the FROG method by implementing a high-resolution spectrometer into the path of the SHG signal, leading to a model-free full-temporal characterization of XFEL pulses.

V. CONCLUSIONS

In conclusion, we succeeded in the hard x-ray intensity autocorrelation measurement with TPA in Zr, using the Si(220) SDO system combined with the reflection self-seeding operation. The autocorrelation trace gave the pulse duration of 7.6 ± 0.8 fs in FWHM for a Gaussian assumption. The temporal shape of the split XFEL pulses with a sharp peak (7.4 fs in FWHM) and oscillatory tail was presented through the numerical simulation, which was consistent with the experimental result. The simulation indicated that the temporal shape was mainly determined by the Bragg diffraction in the crystal optics employed in this paper, irrespective of the chirp in the original XFEL pulse with a wide spectral spike width of >1 eV. In this paper, we provide an important benchmark for a broad range of future developments, such as temporal tailoring of fluctuating x-ray pulses and background-free and full-temporal characterization of XFEL pulses with a pulse duration ranging from 10 as to 100 ps, covering SASE, attosecond, and cavity-based XFELs.

ACKNOWLEDGMENTS

The authors would like to thank all the staffs of SACLA for their continuous supports. This paper was supported by Grant-in-Aid for Early-Career Scientists from Japan Society for the Promotion of Science (JSPS; Grant No. JP18K18307). The experiment was performed at BL3 of SACLA with the approval of Japan Synchrotron Radiation Research Institute (JASRI; Proposal No. 2019A8048).

[1] P. Emma, R. Akre, J. Arthur, R. Bionta, C. Bostedt, J. Bozek, A. Brachmann, P. Bucksbaum, R. Coffee, F.-J. Decker *et al.*, First lasing and operation of an ångstrom-wavelength free-electron laser, Nat. Photon. **4**, 641 (2010).

[2] T. Ishikawa, H. Aoyagi, T. Asaka, Y. Asano, N. Azumi, T. Bizen, H. Ego, K. Fukami, T. Fukui, Y. Furukawa *et al.*, A compact x-ray free-electron laser emitting in the sub-ångström region, Nat. Photon. **6**, 540 (2012).

[3] H.-S. Kang, C.-K. Min, H. Heo, C. Kim, H. Yang, G. Kim, I. Nam, S. Y. Baek, H.-J. Choi, G. Mun *et al.*, Hard x-ray free-electron laser with femtosecond-scale timing jitter, Nat. Photon. **11**, 708 (2017).

[4] W. Decking, S. Abeghyan, P. Abramian, A. Abramsky, A. Aguirre, C. Albrecht, P. Alou, M. Altarelli, P. Altmann, K. Amyan *et al.*, A MHz-repetition-rate hard x-ray free-electron laser driven by a superconducting linear accelerator, Nat. Photon. **14**, 391 (2020).

[5] E. Prat, R. Abela, M. Aiba, A. Alarcon, J. Alex, Y. Arbelo, C. Arrell, V. Arsov, C. Bacellar, C. Beard *et al.*, A compact and cost-effective hard x-ray free-electron laser driven by a high-brightness and low-energy electron beam, Nat. Photon. **14**, 748 (2020).

[6] Z. Huang and K.-J. Kim, Review of x-ray free-electron laser theory, Phys. Rev. ST Accel. Beams **10**, 034801 (2007).

[7] S. Gerber, S.-L. Yang, D. Zhu, H. Soifer, J. A. Sobota, S. Rebec, J. J. Lee, T. Jia, B. Moritz, C. Jia *et al.*, Femtosecond electron-phonon lock-in by photoemission and x-ray free-electron laser, Science **357**, 71 (2017).

[8] K. H. Kim, J. G. Kim, S. Nozawa, T. Sato, K. Y. Oang, T. W. Kim, H. Ki, J. Jo, S. Park, C. Song *et al.*, Direct observation of

bond formation in solution with femtosecond x-ray scattering, Nature (London) **518**, 385 (2015).

[9] K. Tamasaku, E. Shigemasa, Y. Inubushi, T. Katayama, K. Sawada, H. Yumoto, H. Ohashi, H. Mimura, M. Yabashi, K. Yamauchi, and T. Ishikawa, X-ray two-photon absorption competing against single and sequential multiphoton processes, Nat. Photon. **8**, 313 (2014).

[10] H. Yoneda, Y. Inubushi, K. Nagamine, Y. Michine, H. Ohashi, H. Yumoto, K. Yamauchi, H. Mimura, H. Kitamura, T. Katayama, T. Ishikawa, and M. Yabashi, Atomic inner-shell laser at 1.5-ångström wavelength pumped by an x-ray free-electron laser, Nature (London) **524**, 446 (2015).

[11] See, for example, I. A. Walmsley and C. Dorrer, Characterization of ultrashort electromagnetic pulses, Adv. Opt. Photon. **1**, 308 (2009).

[12] R. Mitzner, A. A. Sorokin, B. Siemer, S. Roling, M. Rutkowski, H. Zacharias, M. Neeb, T. Noll, F. Siewert, W. Eberhardt *et al.*, Direct autocorrelation of soft-x-ray free-electron-laser pulses by time-resolved two-photon double ionization of He, Phys. Rev. A **80**, 025402 (2009).

[13] J. A. Armstrong, Measurement of picosecond laser pulse widths, Appl. Phys. Lett. **10**, 16 (1967).

[14] J. A. Giordmaine, P. M. Rentzepis, S. L. Shapiro, and K. W. Wecht, Two-photon excitation of fluorescence by picosecond light pulses, Appl. Phys. Lett. **11**, 216 (1967).

[15] R. Trebino, K. W. DeLong, D. N. Fittinghoff, J. N. Sweetser, M. A. Krumbügel, B. A. Richman, and D. J. Kane, Measuring ultrashort laser pulses in the time-frequency domain using frequency-resolved optical gating, Rev. Sci. Instrum. **68**, 3277 (1997).

[16] H. Yoneda, Y. Inubushi, M. Yabashi, T. Katayama, T. Ishikawa, H. Ohashi, H. Yumoto, K. Yamauchi, H. Mimura, and H. Kitamura, Saturable absorption of intense hard x-rays in iron, Nat. Commun. **5**, 5080 (2014).

[17] M. Fuchs, M. Trigo, J. Chen, S. Ghimire, S. Shwartz, M. Kozina, M. Jiang, T. Henighan, C. Bray, G. Ndabashimiye *et al.*, Anomalous nonlinear x-ray Compton scattering, Nat. Phys. **11**, 964 (2015).

[18] S. Ghimire, M. Fuchs, J. Hastings, S. C. Herrmann, Y. Inubushi, J. Pines, S. Shwartz, M. Yabashi, and D. A. Reis, Nonsequential two-photon absorption from the K shell in solid zirconium, Phys. Rev. A **94**, 043418 (2016).

[19] T. Kroll, C. Weninger, R. Alonso-Mori, D. Sokaras, D. Zhu, L. Mercadier, V. P. Majety, A. Marinelli, A. Lutman, M. W. Guetg *et al.*, Stimulated X-Ray Emission Spectroscopy in Transition Metal Complexes, Phys. Rev. Lett. **120**, 133203 (2018).

[20] S. Shwartz, M. Fuchs, J. B. Hastings, Y. Inubushi, T. Ishikawa, T. Katayama, D. A. Reis, T. Sato, K. Tono, M. Yabashi, S. Yudovich, and S. E. Harris, X-Ray Second Harmonic Generation, Phys. Rev. Lett. **112**, 163901 (2014).

[21] K. Tamasaku, E. Shigemasa, Y. Inubushi, I. Inoue, T. Osaka, T. Katayama, M. Yabashi, A. Koide, T. Yokoyama, and T. Ishikawa, Nonlinear Spectroscopy with X-Ray Two-Photon Absorption in Metallic Copper, Phys. Rev. Lett. **121**, 083901 (2018).

[22] T. Osaka, T. Hirano, Y. Morioka, Y. Sano, Y. Inubushi, T. Togashi, I. Inoue, K. Tono, A. Robert, K. Yamauchi, J. B. Hastings, and M. Yabashi, Characterization of temporal coherence of hard x-ray free-electron laser pulses with single-shot interferograms, IUCrJ **4**, 728 (2017).

[23] D. Zhu, Y. Sun, D. W. Schafer, H. Shi, J. H. James, K. L. Gumerlock, T. O. Osier, R. Whitney, L. Zhang, J. Nicolas *et al.*, Development of a hard x-ray split-delay system at the Linac Coherent Light Source, Proc. SPIE **10237**, 102370R (2017).

[24] Y. Sun, N. Wang, S. Song, P. Sun, M. Chollet, T. Sato, T. B. van Driel, S. Nelson, R. Plumley, J. Montana-Lopez *et al.*, Compact hard x-ray split-delay system based on variable-gap channel-cut crystals, Opt. Lett. **44**, 2582 (2019).

[25] G. Grübel, G. B. Stephenson, C. Gutt, H. Sinn, and Th. Tschentscher, XPCS at the European x-ray free electron laser facility, Nucl. Instrum. Methods Phys. Res. B **262**, 357 (2007).

[26] Y. Shinohara, T. Osaka, I. Inoue, T. Iwashita, W. Dmowski, C. W. Ryu, Y. Sarathchandran, and T. Egami, Split-pulse x-ray photon correlation spectroscopy with seeded x-rays from x-ray laser to study atomic-level dynamics, Nat. Commun. **11**, 6213 (2020).

[27] Y. Inubushi, K. Tono, T. Togashi, T. Sato, T. Hatsui, T. Kameshima, K. Togawa, T. Hara, T. Tanaka, H. Tanaka, T. Ishikawa, and M. Yabashi, Determination of the Pulse Duration of an X-Ray Free Electron Laser Using Highly Resolved Single-Shot Spectra, Phys. Rev. Lett. **109**, 144801 (2012).

[28] Y. Inubushi, I. Inoue, J. Kim, A. Nishihara, S. Matsuyama, H. Yumoto, T. Koyama, K. Tono, H. Ohashi, K. Yamauchi, and M. Yabashi, Measurement of the x-ray spectrum of a free electron laser with a wide-range high-resolution single-shot spectrometer, Appl. Sci. **7**, 584 (2017).

[29] C. Gutt, P. Wochner, B. Fischer, H. Conrad, M. Castro-Colin, S. Lee, F. Lehmkhler, I. Steinke, M. Sprung, W. Roseker *et al.*, Single Shot Spatial and Temporal Coherence Properties of the SLAC Linac Coherent Light Source in the Hard X-Ray Regime, Phys. Rev. Lett. **108**, 024801 (2012).

[30] C. Behrens, F.-J. Decker, Y. Ding, V. A. Dolgashev, J. Frisch, Z. Huang, P. Krejcik, H. Loos, A. Lutman, T. J. Maxwell *et al.*, Few-femtosecond time-resolved measurements of x-ray free-electron lasers, Nat. Commun. **5**, 3762 (2014).

[31] I. Inoue, T. Hara, Y. Inubushi, K. Tono, T. Inagaki, T. Katayama, Y. Amemiya, H. Tanaka, and M. Yabashi, X-ray Hanbury Brown-Twiss interferometry for determination of ultrashort electron-bunch duration, Phys. Rev. Accel. Beams **21**, 080704 (2018).

[32] I. Inoue, K. Tamasaku, T. Osaka, Y. Inubushi, and M. Yabashi, Determination of x-ray pulse duration via intensity correlation measurements of x-ray fluorescence, J. Synchrotron Rad. **26**, 2050 (2019).

[33] N. Hartmann, G. Hartmann, R. Heider, M. S. Wagner, M. Ilchen, J. Buck, A. O. Lindahl, C. Benko, J. Grünert, J. Krzywinski *et al.*, Attosecond time-energy structure of x-ray free-electron laser pulses, Nat. Photon. **12**, 215 (2018).

[34] J. Amann, W. Berg, V. Blank, F.-J. Decker, Y. Ding, P. Emma, Y. Feng, J. Frisch, D. Fritz, J. Hastings *et al.*, Demonstration of self-seeding in a hard-x-ray free-electron laser, Nat. Photon. **6**, 693 (2012).

[35] I. Inoue, T. Osaka, T. Hara, T. Tanaka, T. Inagaki, T. Fukui, S. Goto, Y. Inubushi, H. Kimura, R. Kinjo *et al.*, Generation of narrow-band x-ray free-electron laser via reflection self-seeding, Nat. Photon. **13**, 319 (2019).

[36] K. Tono, T. Togashi, Y. Inubushi, T. Sato, T. Katayama, K. Ogawa, H. Ohashi, H. Kimura, S. Takahashi, K. Takeshita *et al.*, Beamline, experimental stations and photon beam diagnostics

for the hard x-ray free electron laser of SACLA, New. J. Phys. **15**, 083035 (2013).

[37] See Supplemental Material at http://link.aps.org/supplemental/10.1103/PhysRevResearch.4.L012035 for the details of the reflection self-seeding mode of operation, the split-delay optical system, and examples of detector images, which includes Refs. [38–43].

[38] T. Osaka, I. Inoue, R. Kinjo, T. Hirano, Y. Morioka, Y. Sano, K. Yamauchi, and M. Yabashi, A micro channel-cut crystal x-ray monochromator for a self-seeded hard x-ray free-electron laser, J. Synchrotron Rad. **26**, 1496 (2019).

[39] S. Matsumura, T. Osaka, I. Inoue, S. Matsuyama, M. Yabashi, K. Yamauchi, and Y. Sano, High-resolution micro channel-cut crystal monochromator processed by plasma chemical vaporization machining for a reflection self-seeded x-ray free-electron laser, Opt. Express **28**, 25706 (2020).

[40] T. Hirano, T. Osaka, Y. Sano, Y. Inubushi, S. Matsuyama, K. Tono, T. Ishikawa, M. Yabashi, and K. Yamauchi, Development of speckle-free channel-cut crystal optics using plasma chemical vaporization machining for coherent x-ray applications, Rev. Sci. Instrum. **87**, 063118 (2016).

[41] K. Tono, T. Kudo, M. Yabashi, T. Tachibana, Y. Feng, D. Fritz, J. Hastings, and T. Ishikawa, Single-shot beam-position monitor for x-ray free-electron laser, Rev. Sci. Instrum. **82**, 023108 (2011).

[42] T. Hirano, T. Osaka, Y. Morioka, Y. Sano, Y. Inubushi, T. Togashi, I. Inoue, S. Matsuyama, K. Tono, A. Robert *et al.*, Performance of a hard x-ray split-and-delay optical system with a wavefront division, J. Synchrotron Rad. **25**, 20 (2018).

[43] S. Shastri, P. Zambianchi, and D. Mills, Dynamical diffraction of ultrashort x-ray free-electron laser pulses, J. Synchrotron Rad. **8**, 1131 (2001).

[44] H. Yumoto, H. Mimura, T. Koyama, S. Matsuyama, K. Tono, T. Togashi, Y. Inubushi, T. Sato, T. Tanaka, T. Kimura *et al.*, Focusing of x-ray free-electron laser pulses with reflective optics, Nat. Photon. **7**, 43 (2013).

[45] T. Kameshima, S. Ono, T. Kudo, K. Ozaki, Y. Kirihara, K. Kobayashi, Y. Inubushi, M. Yabashi, T. Horigome, A. Holland *et al.*, Development of an x-ray pixel detector with multi-port charge-coupled device for x-ray free-electron laser experiments, Rev. Sci. Instrum. **85**, 033110 (2014).

[46] T. Katayama, T. Hirano, Y. Morioka, Y. Sano, T. Osaka, S. Owada, T. Togashi, and M. Yabashi, X-ray optics for advanced ultrafast pump-probe x-ray experiments at SACLA, J. Synchrotron Rad. **26**, 333 (2019).

[47] F. Livet, F. Bley, J. Mainville, R. Caudron, S. G. J. Mochrie, E. Geissler, G. Dolino, D. Abernathy, G. Grübel, and M. Sutton, Using direct illumination CCDs as high-resolution area detectors for x-ray scattering, Nucl. Instrum. Meth. A **451**, 596 (2000).

[48] I. Inoue, Y. Inubushi, T. Osaka, J. Yamada, K. Tamasaku, H. Yoneda, and M. Yabashi, Shortening X-Ray Pulse Duration via Saturable Absorption, Phys. Rev. Lett. **127**, 163903 (2021).

[49] A. Authier, *Dynamical Theory of X-Ray Diffraction* (Oxford University Press, Oxford, 2001).

[50] S. Roling, H. Zacharias, L. Samoylova, H. Sinn, Th. Tschentscher, O. Chubar, A. Buzmakov, E. Schneidmiller, M. V. Yurkov, F. Siewert, S. Braun, and P. Gawlitza, Time-dependent wave front propagation simulation of a hard x-ray split-and-delay unit: towards a measurement of the temporal coherence properties of x-ray free electron lasers, Phys. Rev. ST Accel. Beams **17**, 110705 (2014).

[51] S. Huang, Y. Ding, Y. Feng, E. Hemsing, Z. Huang, J. Krzywinski, A. A. Lutman, A. Marinelli, T. J. Maxwell, and D. Zhu, Generating Single-Spike Hard X-Ray Pulses with Nonlinear Bunch Compression in Free-Electron Lasers, Phys. Rev. Lett. **119**, 154801 (2017).

[52] K.-J. Kim, Yu. Shvyd'ko, and S. Reiche, A Proposal for an X-Ray Free-Electron Laser Oscillator with an Energy-Recovery Linac, Phys. Rev. Lett. **100**, 244802 (2008).

[53] G. Marcus, A. Halavanau, Z. Huang, J. Krzywinski, J. MacArthur, R. Margraf, T. Raubenheimer, and D. Zhu, Refractive Guide Switching a Regenerative Amplifier Free-Electron Laser for High Peak and Average Power Hard X Rays, Phys. Rev. Lett. **125**, 254801 (2020).

[54] H. Johann, Die Erzeugung lichtstarker Röntgenspektren mit Hilfe von Konkavkristallen, Z. Phys. **69**, 185 (1931).

[55] T. Johansson, Über ein neuartiges, genau fokussierendes Röntgenspektrometer, Z. Phys. **82**, 507 (1933).

[56] K. D. Irwin and G. C. Hilton, *Transition-Edge Sensors* (Springer, Berlin Heidelberg, 2005).

[57] J. Yamada, S. Matsuyama, R. Hirose, Y. Takeda, Y. Kohmura, M. Yabashi, K. Omote, T. Ishikawa, and K. Yamauchi, Compact full-field hard x-ray microscope based on advanced Kirkpatrick-Baez mirrors, Optica **7**, 367 (2020).

[58] F. Salin, P. Georges, G. Roger, and A. Brun, Single-shot measurement of a 52-fs pulse, Appl. Opt. **26**, 4528 (1987).